CHEMISTRY OF MATERIALS

Article

pubs.acs.org/cm

Nitrogen Enriched Porous Carbon Spheres: Attractive Materials for Supercapacitor Electrodes and CO_2 Adsorption

Nilantha P. Wickramaratne,[†] Jiantie Xu,[‡,§] Min Wang,[‡] Lin Zhu,[‡] Liming Dai,[‡] and Mietek Jaroniec*[,†]

[†]Department of Chemistry and Biochemistry, Kent State University, Kent, Ohio 44242, United States

[‡]Department of Macromolecular Science and Engineering, Case Western Reserve University, Cleveland, Ohio 44106, United States

[§]Institute for Superconducting and Electronic Materials, University of Wollongong, Wollongong, NSW 2522, Australia

Supporting Information

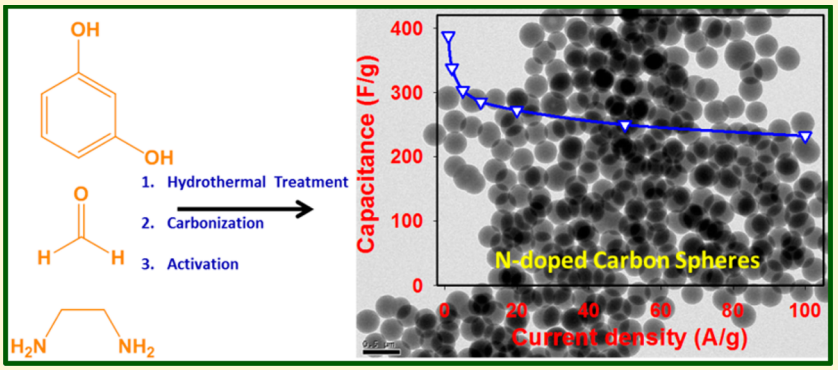

ABSTRACT: A series of nitrogen-containing polymer and carbon spheres were obtained by the sol−gel method. In particular, the nitrogen-rich carbon spheres were prepared by one-pot hydrothermal synthesis in the presence of resorcinol/formaldehyde as carbon precursors and ethylenediamine (EDA) as both a base catalyst and nitrogen precursor, followed by carbonization in nitrogen and activation with CO_2. The introduction of EDA to the sol−gel system resulted in structurally bonded nitrogen-containing carbon spheres. The nitrogen doping level and the particle size can be tuned by varying the EDA amount in the reaction mixture. The maximum nitrogen doping level of 7.2 wt % in carbon spheres could be achieved without sacrificing the spherical morphology. The diameter of these carbon spheres (CS) can be tuned in the rage of 50−1200 nm by varying the EDA amount. N_2 adsorption analysis showed that the aforementioned activated carbon spheres exhibited high surface area reaching up to1224 m^2/g. Ultra high CO_2 adsorption capacities, 4.1 and 6.2 mmol/g, corresponding to an equilibrium pressure of 1 bar, were measured on nitrogen-containing activated carbon spheres at 25 and 0 °C, respectively. Electrochemical measurements performed on these carbon spheres for double layer capacitors showed very high capacitance up to ∼388 F/g at 1.0 A/g, outstanding rate capability (60% capacitance retention at 100 A/g), and unprecedented cycling stability (∼98% capacitance retention even after 8000 cycles) in 1 M H_2SO_4 electrolyte solution.

INTRODUCTION

During the past decade, nitrogen-containing porous carbon materials have been actively studied because of their potential applications in energy storage, catalysis, and adsorption.[1−5] In order to extend the range of their applications, numerous strategies have been employed for fine-tuning of physical and chemical properties of these carbonaceous materials. For instance, activation and doping have been intensively studied for altering the physical and chemical properties of carbons. Moreover, the morphology is also a crucial factor for some applications. For example, spherical particles have been vastly studied for biomedical applications. Thus, the carefully designed carbon materials have shown superior performance in the range of applications, including supercapacitors, fuel cell, solar cells, Li-ion batteries, CO_2 capture, heavy metal adsorption, photocatalysis, and biomedicine.[6−9]

It has been shown that nitrogen doping of carbons can enhance the surface properties, namely surface polarity, electric conductivity, and electron-donor affinity.[10,11] Thus, the nitrogen-containing carbons are potential candidates for energy storage applications and CO_2 capture. Previous studies have also revealed that these carbons can selectively adsorb CO_2 over N_2.[12] Further, it has been shown that these carbons displayed very high initial isosteric heats of CO_2 adsorption (Q_{st}), mainly due to the presence of nitrogen in the carbon matrix. On the other hand, it has also been shown that the nitrogen content in carbon materials is not responsible for physical adsorption of CO_2, but it determines its basicity and, consequently, chemical adsorption of CO_2.[10] In terms of

Received: January 17, 2014
Revised: April 1, 2014
Published: April 2, 2014

   dx.doi.org/10.1021/cm5001895 | Chem. Mater. 2014, 26, 2820−2828

supercapacitors, it has been shown that the capacitance can be dramatically enhanced by nitrogen doping and activation of carbons. However, the physical mechanism(s) behind this capacitance enhancement due to nitrogen doping is not yet fully understood.[13,14] Recently, Zhan et al. showed that nitrogen doping altered the electronic structure of carbon and thus an increase in both charge carrier density and quantum capacitance, leading to a larger interfacial capacitance.[15]

The synthesis of nitrogen-doped porous carbons has been achieved by mainly three methods: (1) the use of nitrogen-containing commercially available monomers (melamine, pyrrole, acetonitrile, 1-butyl-3-methylimidazolium dicyanamide; ionic liquids and polyaniline) as the starting precursors in both nanocasting and soft-templating methods,[3,16] (2) the use of nitrogen-containing biomass and waste products as the starting precursors,[17,18] and (3) the post-treatment of carbons with ammonia and urea[19,20] at elevated temperatures. Among them, the first two methods have been commonly used for the synthesis of nitrogen-containing carbons, mainly due to their easy synthesis and industrial feasibility.

Despite the great efforts in the synthesis of nitrogen-containing porous carbons, there are only a few reports on the preparation of nitrogen-doped porous carbon spheres.[16] One of them is devoted to the synthesis of N-doped carbon nanospheres with a diameter around 80−100 nm and their testing as electrodes for supercapacitors.[21] Interestingly, activation of these N-doped carbon nanospheres showed comparatively high gravimetric capacitance up to 240 F/g in H_2SO_4 electrolyte at 100 mV/s scan rate. However, these activated N-doped carbon nanospheres possessed the specific surface area of 1080 m^2/g and contained only 2.2 wt % of nitrogen atomic weight percent. Another work reported the use of benzoxazine for the synthesis of nitrogen-containing carbon spheres, but these CS featured also a very low atomic percent of nitrogen (2.2 atom %).[22] It was previously shown that the Stöber-like synthesis can be employed for the preparation of sulfur- and nitrogen-containing polymer and carbon spheres in the presence of cysteine, which acts as both a heteroatom precursor and particle stabilizer. These polymer spheres (PS) exhibited comparatively high nitrogen and sulfur contents, 3.1 and 5.4 atom %, respectively. However, CS obtained from these PS possessed a moderate surface area (~670 m^2/g) and exhibited only a trace amount of nitrogen (~1%) and no detectable sulfur, mainly due to the decomposition of heteroatom-containing groups during carbonization at elevated temperatures.[23]

Recent experimental studies have shown that the small-sized microporous carbon spheres exhibited a larger capacitance and better rate performance as compared to larger carbon spheres with similar surface area.[24] It was pointed out that both smaller size and highly monodisperse particles are responsible for reducing mass transport and charge transfer resistance, and for improving the electric double layer capacitor (EDLC) performance. The marked advantage of having microporous carbon spheres with a smaller diameter is that the pores inside the particles are readily accessible to the electrolyte solutions and thus show superior capacitance properties.

Herein, we report the synthesis of nitrogen-containing polymer spheres using the sol−gel method in the presence of EDA as both a catalyst and nitrogen precursor. It is shown that these polymer spheres are nitrogen-rich and their carbonization under nitrogen produced porous CS with unprecedented amount of nitrogen in the carbon matrix up to 7.2 atom %. It is shown that EDA is chemically incorporated to the polymer and carbon structure in the form of pyridinic- and pyrrolic-type nitrogen, which is especially beneficial for the enhancement of the specific capacitance of the resulting carbon spheres. Activation of these carbon spheres under CO_2 gas produced highly porous carbon spheres with a ~1224 m^2/g surface area and comparatively high nitrogen content. Further, a detailed examination of these carbon spheres revealed their potential applications as adsorbents for CO_2 capture and electrode materials for supercapacitors. Namely, the CO_2 adsorption capacity of these CS reached 4.1 and 6.2 mmol/g at 25 and 0 °C, respectively, under atmospheric pressure (1 bar); however, their electrochemical testing for double layer capacitors showed an unprecedented capacitance up to 388 F/g in 1 M H_2SO_4 electrolyte solution at 1 A/g current density.

EXPERIMENTAL SECTION

Synthesis of Nitrogen Containing Polymer/Carbon Spheres. Nitrogen containing PS were synthesized through a one-pot hydrothermal method. Namely, an aqueous-alcoholic solution was prepared by mixing 16 mL of ethanol and 40 mL of distilled water. Subsequently, various amounts of ethylenediamine (EDA, 0.2 to 0.8 mL) were added under continuous stirring. Then, 0.4 g of resorcinol was added and stirred until a complete dissolution occurred. Next, 0.6 mL of 37 wt % formaldehyde was added slowly and stirred for 24 h at 30 °C. Finally, the reaction mixture was transferred to a 125 mL capacity Teflon container and placed in a sealed metal autoclave vessel, which was placed in an oven at 100 °C for 24 h. The solid product (nitrogen containing polymer spheres) was obtained by centrifugation and dried at 100 °C for 12 h. The resulting PS were labeled as PSx where PS refers to polymer spheres, and "x" denotes the EDA amount used (in mL; for instance 1, 2, 3, and 4 refer to 0.2, 0.4, 0.6, and 0.8 mL of EDA, respectively).

In order to obtain nitrogen-doped carbon spheres, N-doped PS were exposed to thermal treatment at 600 °C under a N_2 environment. Thermal treatment in N_2 was performed in flowing nitrogen in the tube furnace using a heating rate of 2 °C/min up to 350 °C, dwelling for 4 h, and heating resumed at a rate of 5 °C/min up to 600 °C, dwelling for 2 h. The resulting carbon spheres were labeled as CSx-T; symbols "x" and "T" refer to the amount of EDA (as mentioned in the notation referring to PS) and the initial digit of the carbonization temperature, respectively, whereas "CS" refers to carbon spheres; for instance, in the case of the CS3−6 sample, CS, 3, and 6 refer to carbon spheres, the EDA amount (3 refers to 0.6 mL of EDA, see above), and carbonization temperature (6 refers to 600 °C, respectively). The postsynthesis activation for carbon spheres was performed by placing a ceramic boat with 0.2 g of CS in a ceramic tube furnace under flowing nitrogen with a heating rate of 10 °C/min up to 850 °C. After reaching the specified temperature, the activating gas was introduced to the tube furnace (50 cm^3/min) for 4 h and then switched back to nitrogen to prevent further activation during the cool down process. The obtained activated materials are denoted as CSx-TA, where "A" refers to activation, which in all cases was performed at 850 °C under carbon dioxide environment for 4 h; the remaining part of the sample notation (CSx-T) is the same as in the case of nonactivated CS (see above).

Characterization of Polymer and Carbon Spheres. TEM (Transmission Electron Microscopy) images were obtained using FEI Tecnai F20ST/STEM instrument operated at 200 keV. The preparation of samples for TEM analysis involved their sonication in ethanol for 2 to 5 min and deposition on a 400 mesh lacy carbon coated copper grid. SEM (Scanning Electron Microscopy) images were obtained using Hitachi S-2600N scanning electron microcopy. Nitrogen adsorption isotherms were measured at −196 °C on ASAP 2010/ASAP 2020 volumetric adsorption analyzers manufactured by Micromeritics (Norcross, GA, USA) using nitrogen of 99.998% purity. Before adsorption measurements, each sample was degassed under a vacuum for at least 2 h at 200 °C. The specific surface area of the

samples was calculated using the Brunauer–Emmett–Teller (BET) method within the relative pressure range of 0.05–0.20. Incremental pore size distributions were obtained from the nitrogen adsorption isotherms by the DFT (Density Functional Theory) method provided by Micromeritics. The thermogravimetric (TG) measurements were performed on a TA Instrument TGA Q500 thermogravimetric analyzer using a high-resolution mode. FT-IR (Fourier Transform Infrared Spectroscopy) spectra were collected using a Bruker Vector 22 FTIR spectrometer in the frequency range of 4000–500 cm^{-1}. Elemental analysis of carbon, nitrogen, sulfur, and hydrogen was obtained using a LECO TruSpec Micro elemental analyzer. XPS (X-ray Photoelectron Spectroscopy) measurements were carried out on a VG Microtech ESCA 2000 using a monochromic Al X-ray source (97.9 W, 93.9 eV).

Electrochemical Measurements. Electrochemical measurements were conducted on a computer-controlled potentiostat (CHI 760C, CH Instrument, USA) with a three-electrode electrochemical cell. The standard three-electrode electrochemical cell was fabricated using glassy carbon with deposited sample as the working electrode, platinum wire as the counter electrode, and Ag/AgCl as the reference electrode. The working electrodes were fabricated as follows: first, 5 mg of the carbon sample was added to 1 mL of DI water/isopropanol (1:1) and then subjected to ultrasonication for an hour. The suspension was dropped onto a glassy carbon electrode. After drying, a Nafion solution (0.5 wt % in isopropanol) was coated on the sample as the binder. All the electrochemical measurements were carried out at 25 °C using a 1 M H_2SO_4 electrolyte. The potentials for electrochemical measurements are reported relative to an Ag/AgCl (saturated KCl) reference electrode and the potential window for cycling was confined between 0 and 0.8 V.

The gravimetric specific capacitance C_g was calculated according to the following equation using the discharge portion of the charge–discharge curves:

$$C_g = \frac{I\Delta t}{(m\Delta V)} = \frac{I}{(m\mathrm{K})}$$

where I, Δt, ΔV, m, and K are the applied current, discharge time, voltage change, the mass of active material, and the slope of the discharge curve, respectively.

RESULTS AND DISCUSSION

Morphology. A series of nitrogen-containing polymer and carbon spheres were synthesized using a sol–gel method in the presence of resorcinol and formaldehyde as carbon precursors, EDA as both nitrogen precursor and catalyst, and ethanol–water as a mixed solvent. The N-doped PS were synthesized by varying the EDA amount. Carbonization of these PS in flowing N_2 produced nitrogen-containing carbon spheres. The SEM and TEM images of the as-synthesized PS, CS, and activated CS are shown in Figures 1, S1, and S2. As can be seen in these figures, all samples showed spherical morphology with relatively narrow particle size distribution (see Table 1 for particle sizes). Interestingly, the particle size of PS is decreasing with increasing amount of EDA. An increase in the EDA amount from 0.2 to 0.4 and 0.6 mL caused a gradual decrease in the average particle size from 1000, 850, and 420 nm, respectively. A further increase in the EDA amount resulted in agglomerated partially spherical particles with sizes around 50–80 nm (see Figures S1 and S2). The presence of smaller particles can be explained by the formation of smaller emulsion droplets containing larger amounts of EDA. A similar effect was observed in the Stöber-like cysteine-assisted synthesis of polymer/carbon spheres.[23] However, there was no visible formation of particles when the amount of EDA increased up to 1.0 mL. The smaller particle sizes of CS as compared to PS are mainly caused by the structure shrinkage during thermal

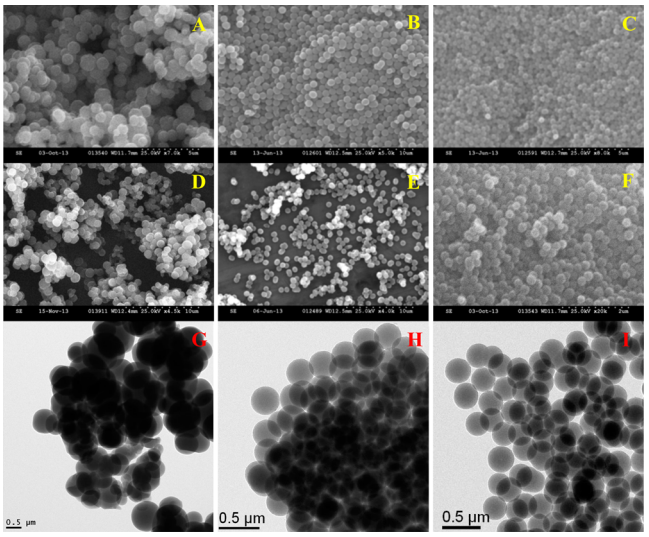

Figure 1. SEM images of (A) CS1–6, (B) CS2–6, (C) CS3–6, (D) CS1–6A, (E) CS2–6A, and (F) CS3–6A and TEM images of CS1–6A (G), CS3–6 (H), and CS3–6A (I).

treatment. Also, the activated CS display even smaller particle sizes than the initial CS, which was mainly caused by peeling off the outer carbon layer during activation with CO_2 at higher temperature and the particle shrinkage; similar behavior was observed during postsynthesis activation of other carbon particles.[25]

Composition and Structure of Polymer and Carbon Spheres. The nitrogen atomic percentage was evaluated by elemental analysis (EA) and X-ray photoelectron spectroscopic (XPS) analysis. The elemental composition (nitrogen atomic %) of the materials studied is provided in Table 1. Data provided in this table show that the nitrogen content in both PS and CS increases with increasing amount of EDA in the reaction mixture. Namely, the nitrogen atomic percentage increased from 6.75 to 10.3% for PS and from 4.1 to 7.2% for CS obtained by varying the amount of EDA from 0.2 to 0.8 mL, respectively. It is evident that both carbonization and activation of PS and CS caused a diminution of nitrogen content in the samples. For instance, the nitrogen atomic percentages are equal to 8.3, 5.0, and 3.55 for PS3, CS3–6, and CS3–6A, respectively. It is noteworthy that the nitrogen loss during carbonization of the polymer studied is smaller as compared to other nitrogen-containing carbons,[23,16] indicating that nitrogen is structurally bonded in the carbon matrix. The type of nitrogen species and the surface elemental composition data obtained by the XPS analysis are shown in Figure 2 and Table 1. The surface N % for PS3 and CS3–6A is 9.1 and 3.8 (at. %), respectively (see Table1). These values are comparable with the EA results, indicating the uniformity of nitrogen distribution throughout the entire particles. As shown in Figure 2, the high resolution XPS spectra (N 1s) further revealed the form of nitrogen in the carbon matrix. The deconvoluted spectra for N 1s with two binding energies 398.2 ± 0.4 and 399.9 ± 0.3 eV correspond to pyridinic, pyrrolic, and/or pyridone-type nitrogen, respectively. It is noteworthy that the signal in the binding energy of the pyridine-type nitrogen for PS3 is higher than that of pyrrolic- and/or pyridone-type nitrogen, indicating the higher concentration of the former. However, high temperature thermal treatments (carbonization and activation) caused the formation of new forms of nitrogen functionalities. The

dx.doi.org/10.1021/cm5001895 | Chem. Mater. 2014, 26, 2820–2828

Table 1. Adsorption Parameters, Gravimetric Capacitance, and Particle Size for the Sample Studied[a]

sample	D_{PR} (nm)	S_{BET} (m^2/g)	N %	C_G (F/g)	CO_2 uptake (mmol/g) 25 °C	CO_2 uptake (mmol/g) 0 °C	PV_{1nm} (cm^3/g)
PS1	600−1200		6.75				
PS2	800−950		7.60				
PS3	400−450		8.25				
PS4			10.30				
CS1−6	500−1000	514	4.10	31	2.5		0.18
CS2−6	750−800	521	4.80	46	2.8		0.18
CS3−6	330−350	530	5.00	106	3.0		0.18
CS4−6	50−100	500	7.20				0.17
CS1−6A	500−950	1224	2.80	242	3.7	5.5	0.36
CS2−6A	700−750	1147	3.05	330	3.9	5.8	0.35
CS3−6A	260−290	1184	3.55	388	4.1	6.2	0.37

[a]Notation: D_{PR} is the particle size range obtained from TEM and SEM images; S_{BET}, the BET specific surface area obtained from the adsorption data in the range of relative presses from 0.05 to 0.2. N% is nitrogen weight percentages in polymer and carbon spheres; C_G, the gravimetric specific capacitance obtained at 1 A/g in 1 M H_2SO_4 solution. $PV_{1\ nm}$ is the volume of micropores below 1 nm.

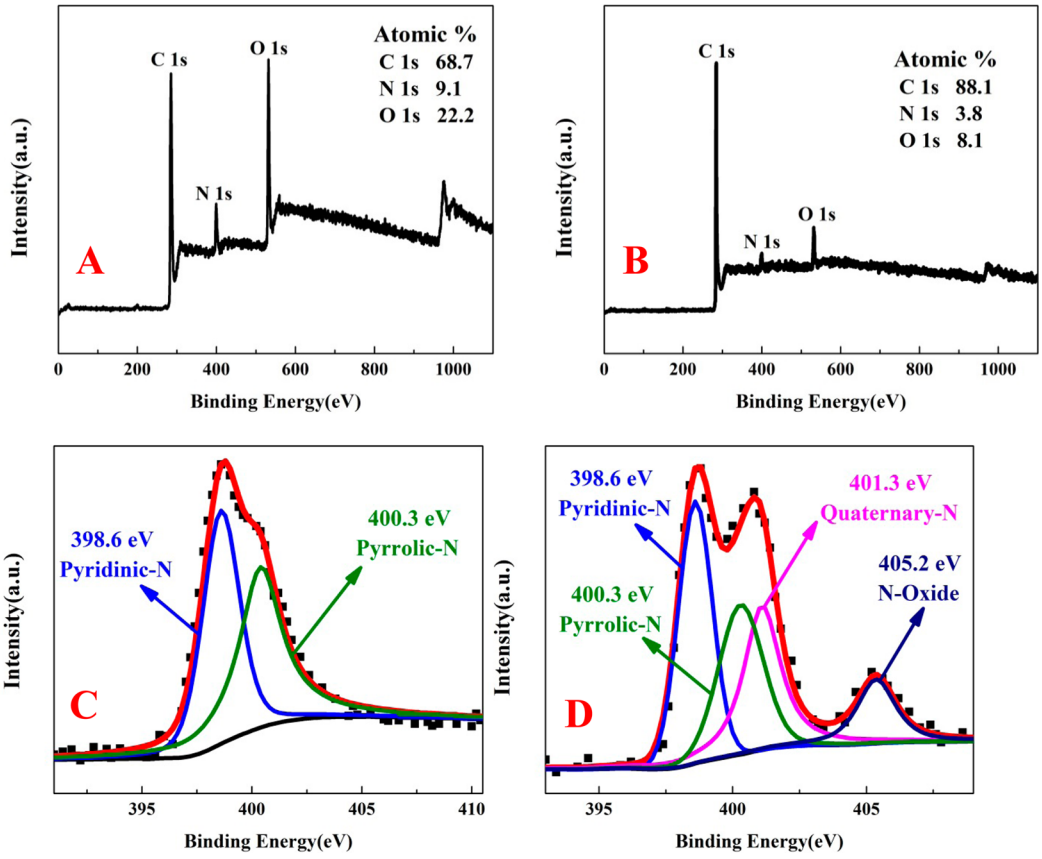

Figure 2. XPS survey spectra of (A) PS3 and (B) CS3−6A and high-resolution XPS spectra of N 1s peak for (C) PS3 and (D) CS3−6A.

deconvoluted XPS spectrum of N 1s for CS3−6A exhibits peaks around 401.3 and 405.2 eV that can be assigned to quaternary nitrogen and pyridinic-N-oxides, respectively. In addition, Figure S3 in the Supporting Information shows the XPS spectrum of O 1s for CS1−6A. The binding energy on this spectrum at 532.0 eV can be associated with phenol (C−OH) and/or ether (C−O−C) groups, while the binding energy at 535.0 eV can be assigned to chemisorbed oxygen, carboxylic groups (COOH), and/or adsorbed water.[32,36] This analysis shows that the activated carbons studied possess mainly phenolic and/or ether-type oxygen functionalities with a negligible amount of other oxygen-containing groups. Of course, the polymer itself contains mainly phenolic and/or ether groups (see Scheme 1), which are preserved to a considerable extent during carbonization and activation processes.

The plausible reaction steps, including vital intermediate molecules, in the formation of a nitrogen containing polymer framework are shown in Scheme 1, which is based on the previously reported reactions of formaldehyde with EDA and resorcinol under basic conditions to form intermediate compounds 4 and 5, respectively.[26,27] This intermediate and the excess of formaldehyde react with resorcinol to form a polymer framework with pyrrolic and pyridinic-type rings. The

dx.doi.org/10.1021/cm5001895 | Chem. Mater. 2014, 26, 2820−2828

Scheme 1. Representation of Possible Resorcinol–Formaldehyde–Ethylenediamine Polymerization

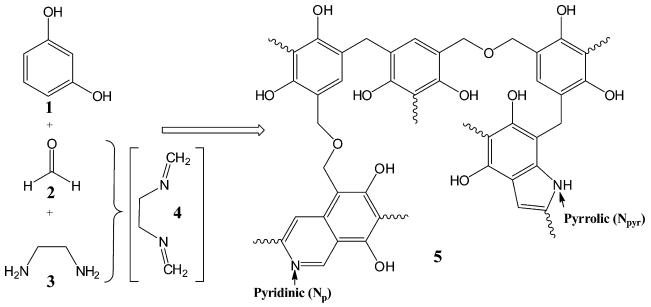

XPS analysis done for PS3 further supports the formation of nitrogen-containing CS outlined in Scheme 1.

A successful incorporation of EDA-formaldehyde derived moieties into a resorcinol-formaldehyde network is also confirmed by FTIR spectra (see Figure S4). Note that the carbonized and activated CS showed similar IR peaks, indicating that both possessed similar functional groups. The peak appearing around 1605 cm^{-1} on the spectrum of PS3 represents the aromatic C=C bond stretching. A small bump appearing around 1659 cm^{-1} on the spectra of both PS and CS corresponds to amine in the pyrrole structure (–NH).[27] Unfortunately, the IR analysis for polymer particles cannot give more details because of the presence of a large number of functional groups such as aldehyde, alcohol, ether, aromatic and aliphatic C=C, etc.; it is difficult to resolve nitrogen-containing functional groups due to the interference from the aforementioned groups. However, carbons possess a smaller number of functional groups, which makes the assignment of IR peaks easier. Thus, strong absorption bands appearing around ~1560 cm^{-1} for CS can be assigned to aromatic C–N stretching[29] with either pyridinic and/or pyrrolic-type nitrogen. This aromatic stretching of C–N in the case of PS3 is stalled due to a broad band for aromatic C=C at 1605 cm^{-1}. A broad absorption peak centered at 1146 cm^{-1} in the case of CS corresponds to the breathing vibration of pyrrole ring.[30]

Nitrogen Adsorption Studies. Nitrogen adsorption isotherms and the corresponding incremental pore size distribution curves obtained for the CS studied at −196 °C are shown in Figures 3 and S5, respectively; panels A and B show nonactivated and activated samples obtained by varying the EDA amount, respectively. All adsorption isotherms except those for CS3–6, CS3–6A, and CS4–6 are type I with a high N_2 adsorption plateau and the absence of hysteresis, indicating the lack of mesopores; however, adsorption isotherms for CS3–6, CS3–6A, and CS4–6 are type IV with distinct hysteresis loops indicating the presence of mesopores, which are created due to the voids between particles. It is clear that the nitrogen adsorption isotherms for the particles below 300 nm show hysteresis, indicating the presence of mesopores, while this hysteresis is not visible for particles lager than 300 nm. The voids between larger particles (>300 nm) are in the macropore range for which adsorption hysteresis is not observed. The incremental pore size distribution curves obtained from N_2 adsorption isotherms by using the density functional theory (DFT) method for slit like pores are shown in Figure S5. All the parameters, specific surface area, and pore structure parameters are listed in Table 1. As shown in Table 1, CS and activated CS possessed the specific surface area ranging from 500 to 552 m^2/g and 1100–1250 m^2/g, respectively. It is obvious that the activated CS possessed a higher surface area, which is mainly due to the creation of a high volume of fine micropores (pore <1 nm) and a relatively high volume of larger micropores (1 nm < pore size < 2 nm) during the high temperature activation process. Namely, the volumes of fine micropores for CS1–6, CS3–6, CS1–6A, and CS3–6A are 0.18, 0.18, 0.36, and 0.37 cm^3/g, respectively.

Electrochemical Studies. The nitrogen doped CSs were used as active materials in the working electrode for electrochemical capacitors in a 1 M H_2SO_4 acidic electrolyte solution. Figures 4 and S6 show the cyclic voltammograms obtained for the CS-6 series of carbons at varying scan rates. These curves were recorded using a three-electrode cell in the potential range from 0 to 0.8 V at various scanning rates. As can be seen from these plots, the CV curves for the nonactivated CS are quasi-rectangular shaped up to a 50 mV/s scan rate, indicating EDLC behavior, and then they are more inclined to the voltage axis with increasing scan rate, indicating a poor capacitive response. The gravimetric specific capacitance of these materials was estimated using the discharge portion of the galvanostatic charge–discharge curves. It is well-known that nitrogen-doped porous carbons are potential materials for supercapacitors mainly due to their wettability toward electrolytes and high conductivity. However, the capacitance values obtained for these carbons at the current density of 1 A/g are ranging from 31 to 106 F/g; namely, these values for CS1–6, CS2–6, and CS3–6 are 31, 46, and 106 F/g, respectively. The gravimetric capacitance obtained for CS3–6 (106 F/g) is higher or comparable to those of the most carbon materials and somewhat lower than values for the most nitrogen-containing carbons under similar electrochemical conditions (see Table

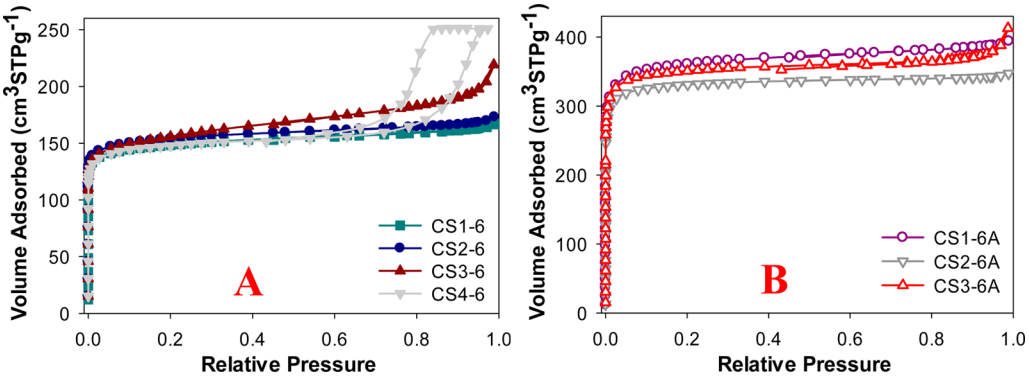

Figure 3. Nitrogen adsorption isotherms for nonactivated CS (A) and activated CS (B).

dx.doi.org/10.1021/cm5001895 | *Chem. Mater.* 2014, 26, 2820–2828

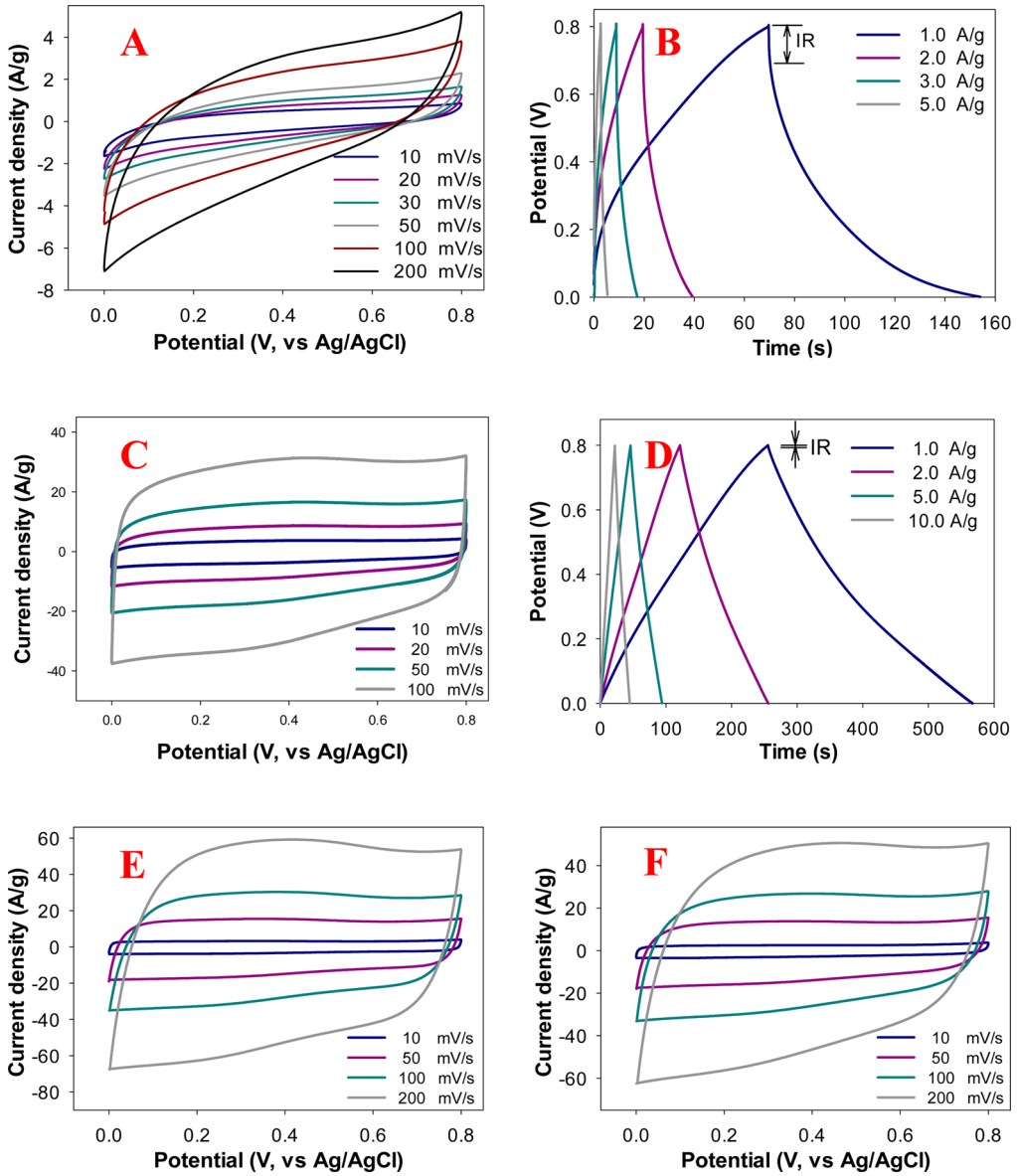

Figure 4. CV and charge−discharge curves for CS3−6 (A, B) and CS3−6A (C, D) and CV curves for CS2−6A (E) and CS1−6A (F).

S1). Thus, this capacitance value is not good enough for the present demand for the clean energy sources with high energy and power densities. These comparatively low capacitances obtained for nonactivated CS (CS-6 series) are mainly due to (1) the low surface area of CS-6 series of carbons and (2) the lack of the accessibility of electrolyte solution to pores of the carbon particle. It is noteworthy that CS3−6 showed the highest capacitance among the CS-6 series of CS, although they have similar specific surface areas. This better performance of CS3−6 can be ascribed to both the particle size and nitrogen-doping. It is evident that the electrolyte solution can penetrate a larger fraction of the pore structure in the case of smaller particles, resulting in higher capacitance. As shown in TEM and SEM images (see Figure 1), the particle size ranges and average particle sizes for the CS3−6, CS2−6, and CS1−6 are 330−350, 750−800, and 500−1000 nm and 340, 760, and 950 nm, respectively. As it was mentioned in the Introduction, the optimization of carbons for supercapacitors can be performed by increasing nitrogen doping and specific surface area.[14] Since the CS studied possessed high nitrogen atomic %, their surface area was enlarged by CO_2 activation.

Activation of the aforementioned nitrogen-doped CS enlarged their surface area without substantial diminution of nitrogen content. As shown in Figures 4D and S7B and D, the galvanostatic charge−discharge curves for the activated CS were used to evaluate the capacitance of the materials studied. The specific capacitances of CS3−6A, CS2−6A, and CS1−6A are 388, 330, and 242 F/g at 1A/g, respectively (see Table 1). As shown in Figures 4B and S6B and D, there is apparently a large internal resistance drop (IR drop) from 0.8 to 0.6 V for all CS samples at 1.0 A/g. However, as compared to CS, activated CS produced nearly symmetrical triangularly shaped galvanostatic charge−discharge curves with a low IR drop [see Figure 4D and S7B and D], indicating less heat waste generation from internal resistance during the cycling.[31] Furthermore, these activated CS showed unprecedented CV performance with rectangular shaped CV curves without leaning the angle even at scan rates as high as 1500 mV/s, 200 mV/s, and 200 mV/s for CS3−6A, CS2−6A, and CS1−6A, respectively, indicating a

dx.doi.org/10.1021/cm5001895 | *Chem. Mater.* 2014, 26, 2820−2828

high capacitive nature with exceptional ion and charge transportation within the electrodes studied (see Figures 4 and S7). It is noteworthy that a small hump observed at ∼0.34 and 0.42 V on the CV curves (Figures 4 and S7) at a low scan rate can be due to redox reactions of the nitrogen-containing groups.[32−34]

The superior cycling performance along with high ion and charge transportation obtained for CS3−6A can be ascribed to the smaller particle size, proper PSD, and heteroatom doping. It can be clearly seen that PSDs for nonactivated CS exhibit single peaks at 0.5−0.6 nm, whereas PSDs for activated CS show multiple peaks centered mainly in 0.5−0.6 nm and 1.0−2.2 nm ranges (see Figure S5). The larger micropores (1.0−2.2 nm) observed in activated CS help to transport ionic electrolyte solution easily through the porous carbon network. One can argue that the highest specific capacitance might come from CS with the highest surface area and proper PSD. Though, CS1−6A exhibited a larger surface area than that of CS3−6A, the latter showed a higher specific capacitance, almost 2 times, which implies that other properties than surface area and PSD govern the ultimate performance of the electrode materials. According to the current study, it is clear that the particle size and nitrogen doping are important factors in determining the capacitance and performance of activated CS as electrode materials for supercapacitors. Two separate reports indicated that smaller carbon particles (∼200 nm) showed higher capacitance up to 196 and 80 F/g at 1 mV/sand 5 mV/s scan rates, respectively.[24,35] The surface areas of these carbons were respectively 800 and 1129 m^2/g. These particles were similar in terms of the size and surface area to the CS3−6A particles. However, CS3−6A showed a much better capacitance performance than the carbons reported elsewhere,[24,35] which was mainly due to the presence of proper nitrogen species such as pyridinic and pyrrolic/pyridone ones and proper PSD (presence of larger micropores). It was shown that pyridinic- and pyrrolic-type nitrogen species as well as quinone-type oxygen species located in pores larger than 1 nm have the most pronounced effect on the capacitance due to the psedocapacitive contribution.[36] Thus, the superior capacitance performance observed for the activated CS studied can be due to the presence of pyridinic- and pyrrolic-type nitrogen as well as proper porosity of the carbon (micropores >1 nm). Moreover, the positively charged quaternary and pyridinic-N-oxides facilitate the transport of electrons throughout the carbon matrix. The possible redox reactions involving pyridinic, pyrrolic, and pyridone-type nitrogen species are shown in Scheme 2.[32−34]

Scheme 2. Possible Redox Reactions Associated Involving Pyridinic, Pyrrolic, and Pyridone-Type Nitrogen Species

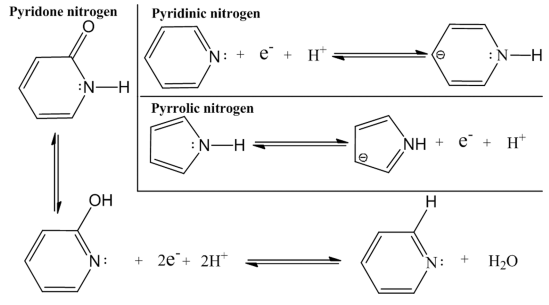

The importance of pore sizes on the performance of carbons as electrodes for supercapacitors can be further illustrated by comparing the capacitance values for CS3−6 and CS3−6A. Even though the CS3−6 carbon possessed a higher percentage of nitrogen (∼5%) than CS3−6A (∼3.5%), its capacitance is much lower than that of CS3−6A at 1 A/g current density. This is mainly due to the absence of larger micropores (>1 nm) in CS3−6, which makes difficult the access of electrolytes to fine pores and heteroatoms and, consequently, reduces the EDL capacitance and pseudocapacitance.

A low CV performance observed for CS1−6A as compared to that of CS3−6A is mainly due to the larger particle size and low nitrogen content in the former. The porous structure of CS1−6A was not completely accessible to electrolyte solution due to its larger particle size; thus, the electrolyte solution did not fully penetrate the particles. This phenomenon can be clearly seen on the basis of the specific capacitance data obtained from the charge−discharge curves (see Figure S7 and Table 1). In addition to the aforementioned pseudocapacitance, nitrogen and oxygen functionalities can also enhance the wettability of the carbon surface to electrolyte solution and, consequently, improve the specific capacitance.

Figure 5A recapitulates the specific capacitance for the activated carbon spheres (ACS) electrodes studied from the galvanostatic charge−discharge curves at different current densities. The capacitance reduction with a simultaneous increase in the current density was mainly due to the increment of diffusion limitation. However, the specific capacitance of CS3−6A at 10, 20, and 100 A/g still preserved a very high capacitance of 285, 272, and 232 F/g, respectively, which corresponds to the capacitance retention of 74, 70 and 60% of the value at 1 A/g. It is also important to note that the capacitance value (388 F/g) obtained for the CS3−6A at 1A/g in 1 M H_2SO_4 is higher than that of many types of nitrogen doped carbon materials, including 3D carbons,[37,38] nanotubes,[39,40] nanocages,[7] nanospheres,[21] graphene,[34,41,42] and nanofibers[43] (see Table S1). To investigate the cycle stability, 8000 consecutive cycles of charge−discharge were recorded for CS3−6A at a current density of 10 A/g. As shown in Figures 5B and S8, there was a fluctuation in the beginning (up to 100 cycles) because of electrode activation and no capacitance loss afterward, indicating the excellent stability of CS3−6A as an electrode for supercapacitors; ∼98% of the original capacitance was preserved even after 8000 cycles. Figure S8B shows that the electrochemical capacitance curve for CS3−6A exhibits almost ideal shape with the imaginary part of the impedance in the low frequency region perpendicular to the real part.

CO_2 Adsorption Studies. It was shown previously that nitrogen containing porous carbons are potential materials for CO_2 adsorption.[4,44] Thus, we have investigated CO_2 adsorption capacities of these porous CS at 25 and 0 °C under atmospheric pressure (1 bar). The CO_2 adsorption isotherms measured under ambient conditions for activated and nonactivated samples are shown in Figure 6. As can be seen from Figure 6A, the CO_2 adsorption capacities for CS are 3.0, 2.8, and 2.5 mmol/g for CS3−6, CS2−6, and CS1−6 and 4.1, 3.9, and 3.7 mmol/g for CS3−6A, CS2−6A, and CS1−6A, respectively, at 25 °C and 1 bar. The increment in the CO_2 adsorption capacity of ACS is mainly due the presence of a large fraction of fine micropores (pore size <1 nm). It was previously shown that physical adsorption of CO_2 on porous carbons under ambient conditions is governed by the volume of fine micropores.[25,45,46] The CS-6 series of carbons possessed similar volumes of

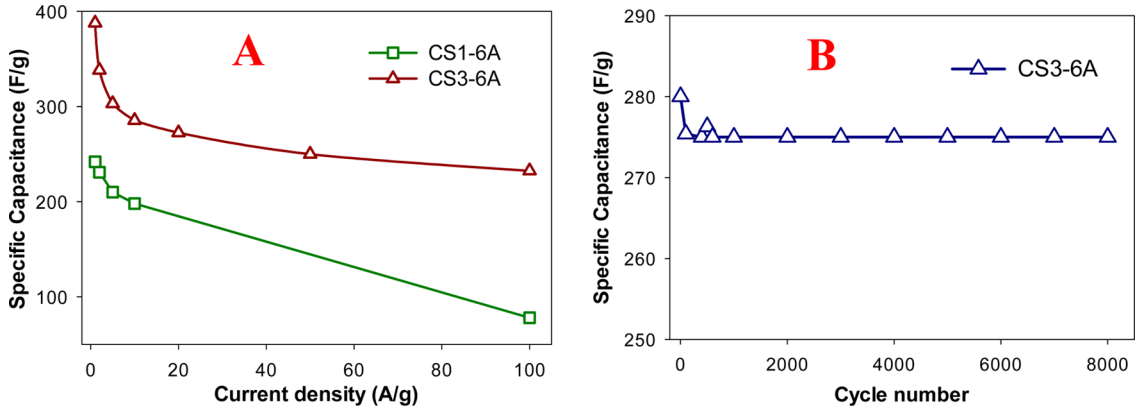

Figure 5. Specific capacitance calculated from galvanostatic charge−discharge curves (A) and cycling stability measured for CS3−6A at 10 A/g in 1 M H_2SO_4 (B).

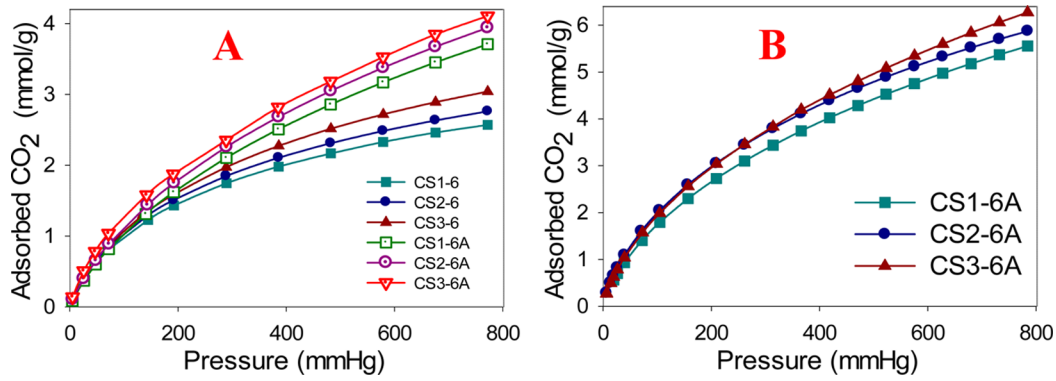

Figure 6. CO_2 adsorption isotherms for the carbon spheres measured at 25 °C (A) and 0 °C (B).

micropores, and one can argue that those three samples might have similar CO_2 capacities. But, it is clearly seen that there was a small CO_2 uptake rise for both CS-6 and CS-6A series with increasing nitrogen doping level, indicating the effect of nitrogen percentage in the CS on CO_2 adsorption. As shown in Figure 6B, the activated CS showed a comparatively high CO_2 uptake of 6.2 and 5.8 mmol/g for CS3−6A and CS2−6A, respectively, at 0 °C and 1 bar. Interestingly, the areal CO_2 uptake obtained for these ACSs using specific CO_2 uptake and the specific surface area of the respective samples are ranging from 5.1 to 5.3 μmol/m^2. Specifically, the areal CO_2 uptakes for CS3−6A and CS2−6A are 5.24 and 5.10 μmol/m^2, respectively, at 0 °C and 1 bar pressure. These values are higher than those of many reported carbons and comparable with the nitrogen containing carbons; for instance, activated phenolic resin-based CS showed only 3.27 μmol/m^2 areal CO_2 uptake,[25] and nitrogen containing CS showed ∼6.0 μmol/m^2 at 0 °C and 1 bar.[47] This very high areal CO_2 uptake for nitrogen doped CS (current samples) is a clear indication of the effect of nitrogen on CO_2 adsorption. Therefore, it can be concluded that the overall CO_2 adsorption of the CS studied is a combination of two contributions: a major contribution related to adsorption in fine micropores and a minor contribution due to adsorption on nitrogen containing basic groups.

CONCLUSIONS

A facile one-pot synthesis of nitrogen-containing polymer spheres was developed. Carbonization and controlled activation of these PS produced nitrogen containing CS with improved surface properties. These activated CS possessed a large fraction of fine micropores, large surface area, and high nitrogen atomic percentage, leading to exceptional electrochemical properties and high CO_2 adsorption capacities. Notably, supercapacitors based on these CS electrodes in 1 M H_2SO_4 electrolyte solution exhibited very high capacitance up to 388 F/g and 232 F/g at 1A/g and 100 A/g, respectively, which corresponds to 60% capacitance retention at 100 A/g of the value at 1A/g. These values are higher than the capacitance reported so far for many carbon-based materials. Further, these carbons showed unprecedented CV performance; namely, CS3−6A showed nearly rectangular shape of the CV curves even at a 3000 mV/s scan rate and very high capacitance retention (98%) even after 8000 cycles. Superior performance of CO_2 activated CS as electrodes for supercapacitors is mainly due to three factors: (1) Smaller particle size and proper PSD facilitate penetration of the electrolyte solution through the particles. (2) Nitrogen and oxygen functionalities improve the wettability of the carbon surface, enhancing the accessibility of active surface area to the electrolyte solution, and in addition, (3) pyridinic-, pyrrolic-, and/or pyridone-type nitrogen species generate an additional minor contribution (pseudocapacitance) to EDLC, which originates mainly from high microporosity. Moreover, these nitrogen containing carbon spheres exhibited comparatively high CO_2 adsorption capacities reaching up to 6.2 mmol/g at 0 °C and 1 bar and very high areal uptakes up to 5.24 μmol/m^2.

dx.doi.org/10.1021/cm5001895 | *Chem. Mater.* 2014, 26, 2820−2828

■ ASSOCIATED CONTENT

Supporting Information

Figures presenting SEM images, TEM images, XPS spectrum, pore size distributions, and electrochemical measurements for the samples studied and one table showing a comparison of the specific capacitance values for various carbons. This material is available free of charge via the Internet at http://pubs.acs.org/.

■ AUTHOR INFORMATION

Corresponding Author

*Phone: 330-672-3790. Fax: 330-672-3816. E-mail: jaroniec@kent.edu.

Notes

The authors declare no competing financial interest.

■ ACKNOWLEDGMENTS

The TEM data were obtained at the (cryo) TEM facility at the Liquid Crystal Institute, Kent State University, supported by the Ohio Research Scholars Program Research Cluster on Surfaces in Advanced Materials. The authors thank Dr. Min Gao for technical support with the TEM experiments. We also would like to thank Dr. Yuhua Xue for his kind help in the XPS measurements and partial support from AFOSR (FA9550-12-1-0069, FA9550-12-1-0037).

■ REFERENCES

(1) Chen, L.; Zhang, X.; Liang, H.; Kong, M.; Guan, Q.; Chen, P.; Wu, Z.; Yu, S. *ACS Nano* **2012**, *6*, 7092−7102.
(2) Merlet, C.; Rotenberg, B.; Madden, P. A.; Taberna, P.; Simon, P.; Gogotsi, Y.; Salanne, M. *Nat. Mater.* **2012**, *11*, 306−310.
(3) Qiu, B.; Pan, C.; Qian, W.; Peng, Y.; Qiu, L.; Yan, F. *J. Mater. Chem. A* **2013**, *1*, 6373−6378.
(4) Xing, W.; Liu, C.; Zhou, Z.; - Zhang, L.; Zhou, J.; Zhuo, S.; Yan, Z.; Gao, H.; Wang, G.; Qiao, S. Z. *Energy Environ. Sci.* **2012**, *5*, 7323−7327.
(5) Wang, L.; Yang, R. T. *J. Phys. Chem. C* **2012**, *116*, 1099−1106.
(6) Simon, P.; Gogotsi, Y. *Nat. Mater.* **2008**, *7*, 845−854.
(7) Tan, Y.; Xu, C.; Chen, G.; Liu, Z.; Ma, M.; Xie, Q.; Zheng, N.; Yao, S. *ACS Appl. Mater. Interfaces* **2013**, *5*, 2241−2248.
(8) Hao, G.; Li, W.; Qian, D.; Lu, A. *Adv. Mater.* **2010**, *22*, 853−857.
(9) Wickramaratne, N. P.; Perera, V. S.; Park, B.; Gao, M.; McGimpsey, G. W.; Huang, S. D.; Jaroniec, M. *Chem. Mater.* **2013**, *25*, 2803−2811.
(10) Chen, H.; Sun, F.; Wang, J.; Li, W.; Qiao, W.; Ling, L.; Long, D. *J. Phys. Chem. C* **2013**, *117*, 8318−8328.
(11) Shen, W.; Fan, W. *J. Mater. Chem. A* **2013**, *1*, 999−1013.
(12) Zhong, M.; Natesakhawat, S.; Baltrus, J. P.; Luebke, D.; Nulwala, H.; Matyjaszewski, K.; Kowalewski, T. *Chem. Commun.* **2012**, *48*, 11516−11518.
(13) Zhao, L.; Fan, L.; Zhou, M.; Guan, H.; Qiao, S.; Antonietti, M.; Titirici, M. *Adv. Mater.* **2010**, *22*, 5202−5206.
(14) Wang, J.; Kaskel, S. *J. Mater. Chem.* **2012**, *22*, 23710−23725.
(15) Zhang, L. L.; Zhao, X.; Ji, H.; Stoller, M. D.; Lai, L.; Murali, S.; Mcdonnell, S.; Cleveger, B.; Wallace, R. M.; Ruoff, R. S. *Energy Environ. Sci.* **2012**, *5*, 9618−9625.
(16) Wickramaratne, N. P.; Jaroniec, M. *Adsorption* **2014**, *20*, 287−293.
(17) Zhu, H.; Yin, J.; Wang, X.; Wang, H.; Yang, X. *Adv. Funct. Mater.* **2013**, *23*, 1305−1312.
(18) Li, Z.; Xu, Z.; Tan, X.; Wang, H.; Holt, C. M. B.; Stephenson, T.; Olsen, B. C.; Mitlin, D. *Energy Environ. Sci.* **2013**, *6*, 871−878.
(19) Pietrzak, R.; Wachowska, H.; Nowicki, P. *Energy Fuels* **2006**, *20*, 1275−1280.
(20) Wang, X.; Liu, C.; Neff, D.; Fulvio, P. F.; Mayes, R. T.; Zhamu, A.; Fang, Q.; Chen, G.; Meyer, H. M.; Jang, B. Z.; Dai, S. *J. Mater. Chem. A* **2013**, *1*, 7920−7926.
(21) Su, F.; Poh, C. K.; Chen, J. S.; Xu, G.; Wang, D.; Li, Q.; Lin, J.; Lou, X. W. *Energy Environ. Sci.* **2011**, *4*, 717−724.
(22) Wang, S.; Li, W.; Hao, G.; Hao, Y.; Sun, Q.; Zhang, X.; Lu, A. *J. Am. Chem. Soc.* **2011**, *133*, 15304−15307.
(23) Wickramaratne, N. P.; Perera, V. S.; Ralph, J. M.; Huang, S. D.; Jaroniec, M. *Langmuir* **2013**, *29*, 4032−4038.
(24) Tanaka, S.; Nakao, H.; Mukai, T.; Katayama, Y.; Miyake, Y. *J. Phys. Chem. C* **2012**, *116*, 26791−26799.
(25) Wickramaratne, N. P.; Jaroniec, M. *ACS Appl. Mater. Interfaces* **2013**, *5*, 1849−1855.
(26) Rivera, A.; Ríos-Motta, J. *Tetrahedron Lett.* **2005**, *46*, 5001−5004.
(27) Muylaert, I.; Verberckmoes, A.; De Decker, J.; Van Der Voort, P. *Adv. Colloid Interface Sci.* **2012**, *175*, 39−51.
(28) Li, Z. P.; Liu, Z. X.; Zhu, K. N.; Li, Z.; Liu, B. H. *J. Power Sources* **2012**, *219*, 163−171.
(29) Zhou, H.; Xu, S.; Su, H.; Wang, M.; Qiao, W.; Ling, L.; Long, D. *Chem. Commun.* **2013**, *49*, 3763−3765.
(30) Zhang, D.; Dong, Q.; Wang, X.; Yan, W.; Deng, W.; Shi, L. *J. Phys. Chem. C* **2013**, *117*, 20446−20455.
(31) Wu, Q.; Xu, Y.; Yao, Z.; Liu, A.; Shi, G. *ACS Nano* **2010**, *4*, 1963−1970.
(32) Lee, Y.; Chang, K.; Hu, C. J. *Power Sources* **2013**, *227*, 300.
(33) Frackowiak, E. *Phys. Chem. Chem. Phys.* **2007**, *9*, 1774.
(34) Jeong, H. M.; Lee, J. W.; Shin, W. H.; Choi, Y. J.; Shin, H. J.; Kang, J. K.; Choi, J. W. *Nano Lett.* **2011**, *11*, 2472−2477.
(35) Qiao, Z.; Guo, B.; Binder, A. J.; Chen, J.; Veith, G. M.; Dai, S. *Nano Lett.* **2013**, *13*, 207−212.
(36) Hulicova-Jurcakova, D.; Seredych, M.; Lu, G. Q.; Bandosz, T. J. *Adv. Funct. Mater.* **2009**, *19*, 438−447.
(37) Chen, X. Y.; Chen, C.; Zhang, Z. J.; Xie, D. H.; Deng, X.; Liu, J. W. *J. Power Sources* **2013**, *230*, 50−58.
(38) Dhawale, D. S.; Mane, G. P.; Joseph, S.; Anand, C.; Ariga, K.; Vinu, A. *ChemPhysChem* **2013**, *14*, 1563−1569.
(39) Kaempgen, M.; Chan, C. K.; Ma, J.; Cui, Y.; Gruner, G. *Nano Lett.* **2009**, *9*, 1872−1876.
(40) Mun, Y.; Jo, C.; Hyeon, T.; Lee, J.; Ha, K.; Jun, K.; Lee, S.; Hong, S.; Lee, H. I.; Yoon, S.; Lee, J. *Carbon* **2013**, *64*, 391−402.
(41) Zhu, Y.; Murali, S.; Stoller, M. D.; Ganesh, K. J.; Cai, W.; Ferreira, P. J.; Pirkle, A.; Wallace, R. M.; Cychosz, K. A.; Thommes, M.; Su, D.; Stach, E. A.; Ruoff, R. S. *Science* **2011**, *332*, 1537−1541.
(42) Dong, X.; Xu, H.; Wang, X.; Huang, Y.; Chan-Park, M.; Zhang, H.; Wang, L.; Huang, W.; Chen, P. *ACS Nano* **2012**, *6*, 3206−3213.
(43) Jiang, H.; Lee, P. S.; Li, C. *Energy Environ. Sci.* **2013**, *6*, 41−53.
(44) Yang, H.; Yuan, Y.; Tsang, S. C. E. *Chem. Eng. J.* **2012**, *185−186*, 374−379.
(45) de Souza, L. K. C.; Wickramaratne, N. P.; Ello, A. S.; Costa, M. J. F.; da Costa, C. E. F.; Jaroniec, M. *Carbon* **2013**, *65*, 334−340.
(46) Presser, V.; McDonough, J.; Yeon, S.; Gogotsi, Y. *Energy Environ. Sci.* **2011**, *4*, 3059−3066.
(47) Liu, L.; Deng, Q.; Hou, X.; Yuan, Z. *J. Mater. Chem.* **2012**, *22*, 15540−15548.